Comparative assessment of dislocation density in cyclically deformed austenitic stainless steel determined by X-ray diffraction and hardness tests

A THESIS

Submitted by

BALAKUMAR SHIVA SHRAVAN KUMAR

ROLL NO. 111MM0012

AND

TUSHAR

ROLL NO. 111MM0516

In partial fulfilment of the requirements

for the degree of

BACHELOR OF TECHNOLOGY

Under the esteemed guidance of

PROF. KRISHNA DUTTA

DEPARTMENT OF METALLURGICAL AND MATERIALS ENGINEERING

NATIONAL INSTITUTE OF TECHNOLOGY ROURKELA

ROURKELA-769008

Comparative assessment of dislocation density in cyclically deformed austenitic stainless steel determined by X-ray diffraction and hardness tests

A THESIS

Submitted by

BALAKUMAR SHIVA SHRAVAN KUMAR

ROLL NO. 111MM0012

AND

TUSHAR

ROLL NO. 111MM0516

In partial fulfilment of the requirements

for the degree of

BACHELOR OF TECHNOLOGY

Under the esteemed guidance of

PROF. KRISHNA DUTTA

DEPARTMENT OF METALLURGICAL AND MATERIALS ENGINEERING

NATIONAL INSTITUTE OF TECHNOLOGY ROURKELA

ROURKELA-769008

Certificate

This is to certify that the thesis entitled, **"Comparative assessment of dislocation density in cyclically deformed austenitic stainless steel determined by XRD and hardness tests"** submitted by **Balakumar Shiva Shravan kumar (111MM0012) and Tushar (111MM0516)** in partial fulfillment of the requirements for the award of the degree of **Bachelor of Technology** in **Metallurgical and Materials Engineering** at the **National Institute of Technology, Rourkela** is an authentic work carried out by them under my supervision and guidance. To the best of my knowledge, the matter embodied in the thesis has not been submitted to any other University/ Institute for the award of any degree or diploma.

Date:

Place: Rourkela

Supervisor:

Prof. K. Dutta

Department of Metallurgical and Materials Engineering

National institute of Technology, Rourkela-769008.

Acknowledgements

I take this opportunity to express my deep sense of gratitude and immense respect to my supervisor, Professor K. Dutta, Metallurgical and Materials Engineering Department, NIT Rourkela, for his inspiring guidance, valuable suggestions, and stimulating discussions throughout the research work. It would have been impossible for me to bring out this thesis without his help and constant encouragement.

I am highly grateful to laboratory members of Department of Metallurgical and Materials Engineering, NIT Rourkela, specially Mr. A. Pal of Metallurgy department and Mr.Aravind Sir of MC lab, Ceramic department.

I am thankful to Ms.Keerthi Ravi and Mr. Lala Amarnath of Metallurgy Department for their constant guidance throughout the work.

Finally, I feel great reverence for all my family and friends and the Almighty, for their blessings, and for being a constant source of encouragement.

CONTENT

CHAPTER 3. QUANTITATIVE ESTIMATION

CHAPTER 4. EXPERIMENTAL PROCEDURE

CHAPTER 5. RESULTS AND DISCUSSION

CHAPTER 6. CONCLUSIONS AND FUTURE PROSPECTIVES

Abstract

Among all types of steels, austenitic stainless steel, mostly known for its formability and corrosion resistance, has found its utility in diverse field of applications including pipelines, automobile engine and gear parts. ISO/TR 15510 X12CrMnNiN17-7-5 is a special grade of austenitic stainless steel which was developed to conserve Ni. This non-conventional stainless steel is used in automobile parts such as automotive trim, wheel covers, conveyor belts and railway train bodies etc. In most of these applications, components go through cyclic loading resulting in low cycle fatigue failure. In general, any deformation in metallic systems is controlled by its internal sub-structural variations (dislocation density) and so it is essential to study sub-structural changes in austenitic stainless steel under cyclic loading. Further, it is well known that austenite in stainless steel is metastable upon monotonic and cyclic deformation. In this investigation, strain induced transformation of austenite to martensite using X-Ray diffraction profile analysis has been studied and volume fraction of martensitic and austenitic phases in cyclically deformed specimens under various constant strain amplitudes has been calculated. In order to calculate the dislocation densities and dislocation character in the specimens subjected to cyclic loading under various constant strain amplitudes X-ray diffraction profile analysis using the modified Williamson–Hall equation has been carried out. Estimation of dislocation density has also been done using variation in hardness values of deformed specimens subjected to varying loads incorporating the model of indentation size effect and compared with that of XRD profile analysis. It has been found that dislocation density increases with increase in strain amplitude which implies that non-conventional austenitic stainless steel is cyclically hardenable material. The comparative assessment indicates that both the models can potentially be used to estimate the dislocation density in deformed materials.

LIST OF FIGURES

LIST OF TABLES

CHAPTER 1

INTRODUCTION

Description & background

Stainless steels are a remarkable and extremely versatile family of engineering materials, which are selected primarily for their corrosion and heat resistant properties [1]. All types of stainless steels contain at least 10.5% chromium [2]. Due to formation of chromium oxide at this percent of chromium surface gets covered and protected from corrosion. The various types of stainless steels based on the metallurgical phases present in them are: 1) Ferritic stainless steels 2) Austenitic stainless steels 3) Martensitic stainless steels 4) Duplex steels [2]. Unlike others, austenitic stainless steels these don't have a yield point and hence they show excellent formability. Applications of austenitic stainless steels include gas pipelines, automotive parts, storage tanks, heat exchangers, reactor bodies, pressure tanks etc. These applications involve situations where the material experiences cyclic loading. This cyclic loading causes degradation of mechanical properties and ultimately failure of component termed as fatigue failure. In general fatigue is a problem that affects any structural component or any moving part and it is known that almost 90% of all engineering failures are due to fatigue [3]. Automobile parts (rotating), aircraft wings (air pressure), ships on the sea (wave pressure) are few examples for cyclic loading in moving parts. Cyclic loading may also be due to fluctuating thermal stresses that causes uneven thermal expansions and contractions. For examples chemical and nuclear reactors, heat exchanger vessels, turbines under cyclic temperature conditions etc. Since in such conditions elongation is fixed due to temperature changes, low cycle fatigue which is strain controlled is observed in such cases. Fatigue failure analysis of conventional grades of austenitic stainless steels like 200 series and 300 series have been extensively studied and results have been published. Comparatively very less research has been done in the non-conventional austenitic

stainless steels like X12CrMnNiN17-7-5 and hence it is important that the low cycle fatigue behavior of non-conventional grades be studied.

During cyclic loading, movement of dislocations occur in the plane oriented in such a way that the shear stress is maximum. The off-repeated to and fro motion of dislocations in the fatigue results in intrusions and extrusions on the surface of the material in the form of bands known as persistent slip bands (PSBs) [4]. The name suggests that the slip bands persist even upon electro polishing and other surface polishing techniques. Dislocation density which refers to number of dislocations passing through a unit area of cross section also changes greatly during cyclic loading. Depending upon the material whether it is cyclically hardenable or softenable, the dislocation density increases or decreases respectively [3]. Dislocation density can be measured by chemical techniques like etching, and X-ray diffraction (XRD), transmission electron microscopy (TEM), hardness tests, etc.[5]. Transmission electron microscopy technique is the most convenient way of measuring dislocation density in a material but, the method of sample preparation is time consuming as it requires a very thin sample for the study. Also the microstructural information obtained in TEM is for an extremely small area of the sample, whereas X-ray diffraction and hardness tests can reveal the average data over a relatively larger area of the sample[5]. Peak broadening and indentation-size effect are the concepts behind dislocation density measurements through XRD and hardness tests respectively. As per the knowledge of the current investigators, there exists no reports in the literature which has done a comparative assessment of dislocation density from both XRD and hardness techniques for a non-conventional austenitic stainless steel subjected to low cycle fatigue. In view of this, few samples which were previously deformed under low cycle fatigue conditions were studied for their dislocation density using XRD and hardness tests.

OBJECTIVES:

Main objectives of this investigation and the plans of work can be summarized as follows:

(1) **Microstructural characterization using optical microscope:** This includes a) observing the microstructure of the sample under optical microscope. b) calculation of grain size by length intercept method using the micrographs.

(2) Calculation of volume fraction of various phases using XRD: This includes calculation of volume fraction of α' (martensite) and γ (austenite) phases in the pre-deformed samples by analysing the XRD peaks.

(3) Calculation of dislocation density and their character using XRD: This includes evaluation of dislocation density by analysing the XRD peaks obtained from the deformed samples and considering the various phases of the sample according to their volume fractions calculated. This also includes calculation of the fraction of screw and edge dislocation densities using various diffraction peaks in XRD analysis.

(4) Calculation of dislocation density using Hardness test: This includes calculation of dislocation density using hardness values of the specimen taken at various loads. The obtained dislocation density values by this method are compared with the respective values obtained by the XRD profile analysis.

This thesis contains five chapters:

Chapter 1 contains the introduction to the concept of fatigue and discussion of fatigue failures in non-conventional austenitic stainless steel. A brief description of dislocations and dislocation density formed in cyclic loading. Various techniques to calculcate dislocation

density and their pros and cons were also mentioned. C**hapter 2** discusses the background theory and literature on the research done in this area. **Chapter 3** contains the theory and formulae required for quantitative estimation of dislocation density through various procedures adopted. **Chapter 4** contains the various experiment done and the procedures are explained in detail. **Chapter 5** comprises of the results obtained in the calculations and discussion on the results including reasons behind various observations. **Chapter 6** contains conclusions drawn from the observations and also includes the future prospectives that are possible for this project work.

CHAPTER 2

LITERATURE REVIEW

2.1 Strain induced martensitic transformation

Martensitic transformation is known to be triggered by either thermal gradient or stress gradient. The strain hardening rate which is interpreted by dislocation density is known to closely depend upon the amount of (α' martensite) formed during deformation **[22].** The amount of α' martensite formed is seen to depend upon deformation mechanisms, plstic strain and deformation methods. Stacking fault energy is the most important factor in controlling the deformation mechanism during deformation. Stacking faut energy is a function of alloy composition and temperature. As the stacking fault energy increases the deformation mode shifts from ε-martensite formation to deformation twinning and slip. Also different applied stress are seen to change the nucleation rate of α'- marensite and hence the resulting microstructure. It is reported that larger volume fractions of α'-martensite is formed in biaxial tension than uniaxial tension due to more intersection of shear bands in biaxial than uniaxial tension **[22]**. Whereas when compressive stresses are applied the austenite to martensite transformation is seen to be suppressed **[22].** Two possible sequences of transformations can occur during deformation in the austenitic stainless steel – (1) γ austenite → mechanically twinned γ' → α' martensite and (2) γ austenite → ε-martensite → α' martensite. Thus there can be two types of martensite that can be formed namely ε-martensite and α-martensite. ε-martensite is a paramagnetic phase just as austenite and it has a hexagonal close pack structure. α'-marensite is ferromagnetic and has body central tetragonal structure. It has the crystal lattice parameters as ferrite phase. The amount of martensite formed upon deformation depends upon various factors such as: material composition, temperature, plastic strain, strain rate, stress state, deformation mode, grain size, grain orientation, etc. The energy required for martensitic transformation is given by plastic deformation. Also there is a temperature M_d above which martensitic transformation cannot

occur by deformation. The stress required for start of transformation decreases with temperature below M_d and becomes zero at M_s (martensitic start temperature). Thus below M_s temperature the transformation is spontaneous. The dependence of this M_d temperature on composition is studied [22] and formulated as follows:

$$M_d = 413 - 13.7(\%Cr) - 9.5(\%ni) - 8.1(\%mn) - 18.5(\%mo) - 9.2\,(\%si) - 462\,(\%[C + n])$$

2.2 DISLOCATIONS

Dislocation is the linear defect due to absence of a row of atoms or presence of half plane of atoms in the lattice. The line along which the half plane of atoms ends is termed as the dislocation and the arrangement of atoms changes below this half plane. If a plane is considered along which slip is of the highest possibility, the dislocation can be observed to be the boundary between the slipped and the unslipped portions of the slip plane [20]. Dislocations are found to be responsible for plastic deformation as observed by transmission electron microscopy. The movement of dislocations is found to be responsible for the differences between the value of theoretical cohesive strength of materials and the practical values of strength. Dislocations are the reason for the materials to deform without failure as the movement of dislocations takes place at a much lesser value of stress compared to sliding of an atomic layer over the one below it. All crystalline materials usually contain dislocations running throughout each crystal or grain and there is usually about 10^{10} to 10^{12} m of dislocation line in a meter cube of material[20]. Dislocations in a material can be revealed by chemical techniques like etching and precipitation and by detecting physical structure around the dislocation using techniques like Transmission electron microscopy and X-ray Diffraction.

2.2.1 TYPES OF DISLOCATIONS: EDGE AND SCREW

There are two different types of dislocations: edge and screw dislocations. The lattice surrounding these dislocations is distorted from the regular periodicity. Edge dislocation was proposed by Orowan, Polanyi, and taylor in the year 1934 [20]. The edge dislocation can be visualized as the line (perpendicular to plane of paper) at which an extra half plane of atoms are terminating Fig.2.1. As can be seen in the Fig.2.11 (b), edge dislocation line AB is the boundary between the slipped region (to the left of ABCD) and the unslipped region (to the right of ABCD).

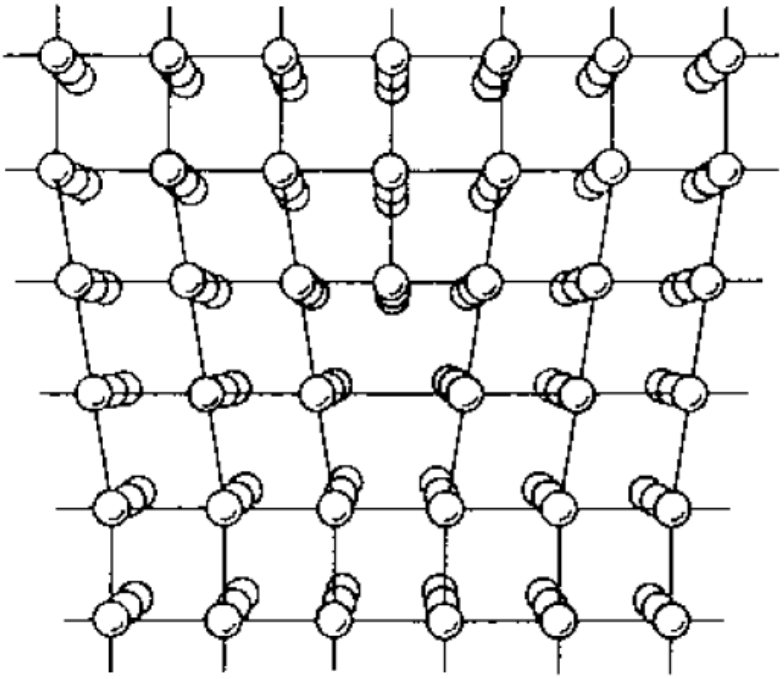

Fig.2.1 Schematic diagram of edge dislocation. (taken from Hirth and Lothe).

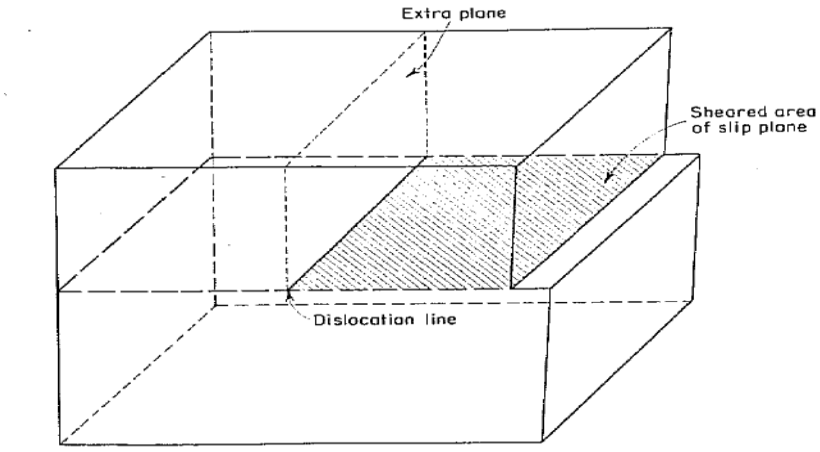

Fig 2.2 The three-dimensional view of crystal containing an edge dislocation that shows dislocation forms a boundary between slipped and unslipped regions.

Screw dislocation was proposed by Burgers in 1939 [21]. The screw dislocation can be visualized by considering the shear displacement of the upper half of the crystal above the slip plane over the lower half. Screw dislocation line is the boundary between slipped region (right of AB) and

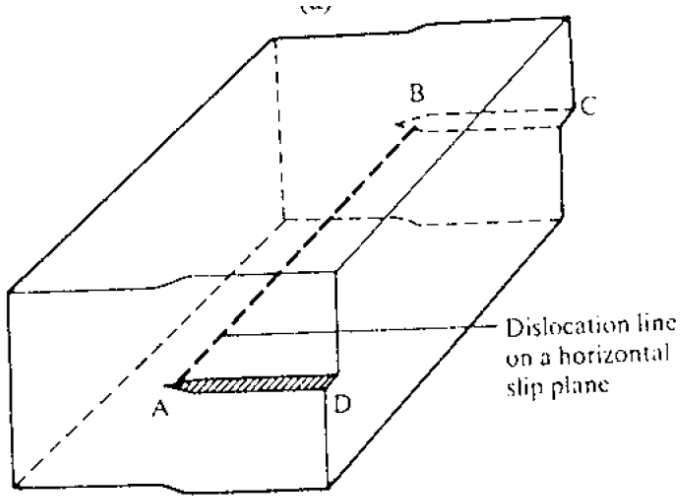

Fig2.3. Schematic diagram showing a screw dislocation and the displacement of upper half over the lower half.

unslipped region (left of AB). It can be also magined as “parking garage” driving around the dislocation line will go up or down the building. It can also be compared to a screw, right or left handed according to right-handed or left handed screw dislocation.

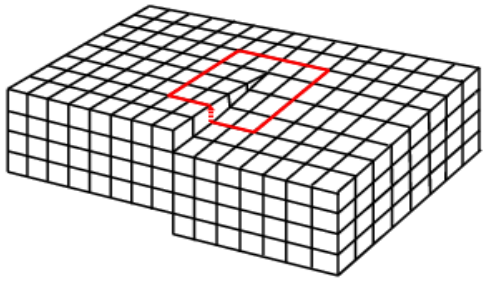

Fig.2.4. Schematic diagram of screw dislocation in a crystal showing atomic arrangement around the dislocation line.

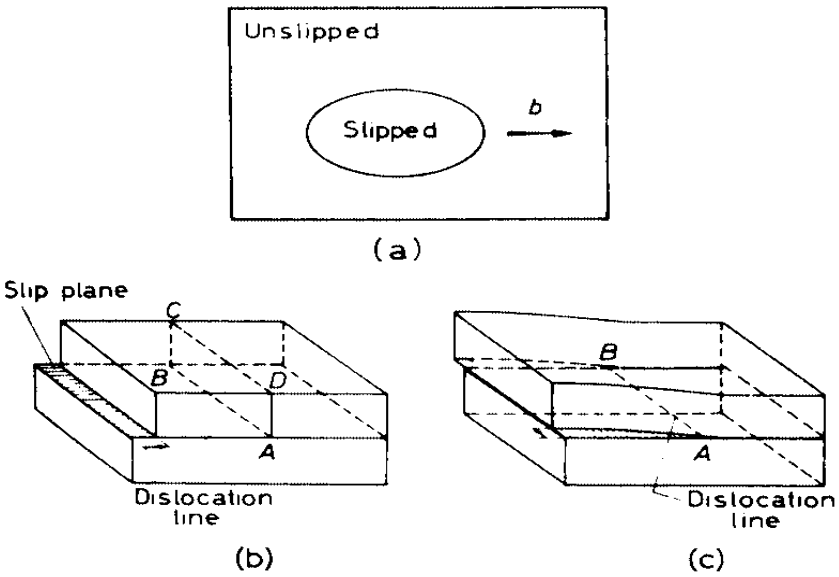

Fig.2.5. Schematic diagram showing a) dislocation as the boundary between slipped and unslipped regions b) edge dislocation c) screw dislocation

In reality most dislocations have both edge and screw characters. A typical mixed dislocation is shown in Fig.2.6. in which it can be seen that at A the character of dislocation is completely screw and at B it is completely edge. The portion of dislocation between A and B is partially edge and partially screw. They are therefore mixed dislocations.

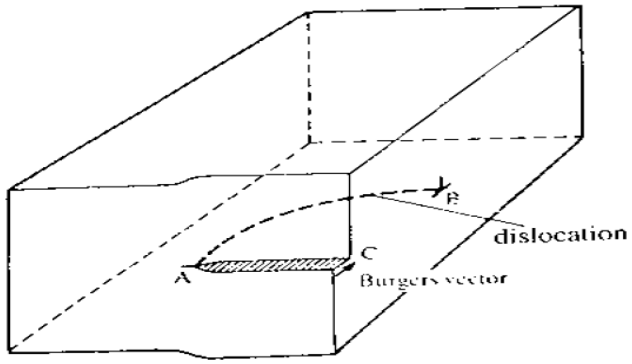

Fig.2.6. Schematic diagram showing mixed dislocation and portions with complete screw (point A) and complete edge (point B)

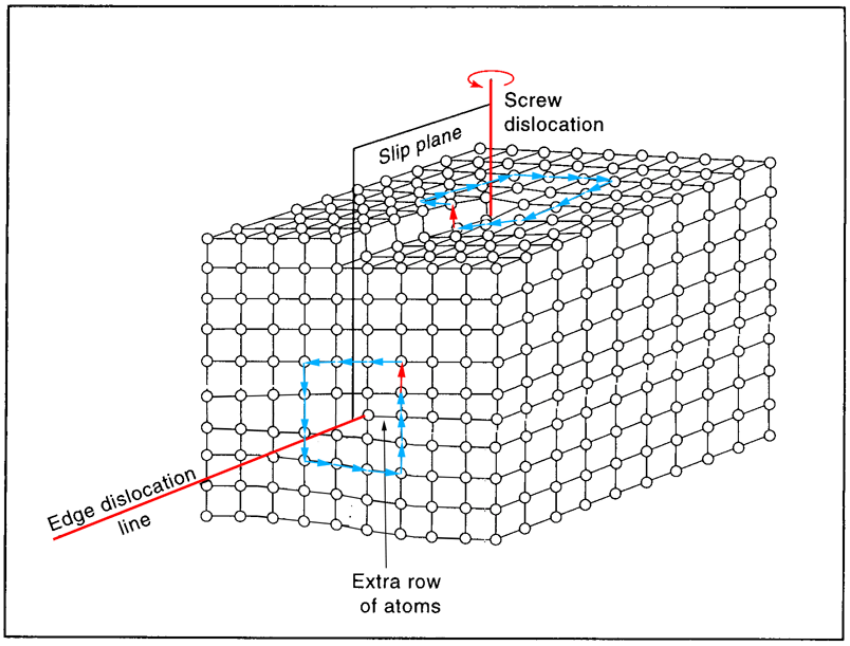

Fig.2.7. Schematic diagram showing atomic arrangement in the lattice around edge and screw dislocation portions of a mixed dislocation.

2.3 DISLOCATION DENSITY:

Dislocation Density is a representation of number of dislocations present in a quantity of material[20]. Dislocation being a line defect, can be defined as the total length of dislocations per unit volume and hence the units are $m/m^3 = m^{-2}$ [21]. It quantifies the number of dislocations crossing a unit area of crosssection. Dislocation density is generally of the order of 10^{10} m^{-2} in ordinary metal, while it increases to $10^{15} m^{-2}$ after work hardening and decreases to around 10^6 m^{-2} upon annealing[21]. Dislocation density increases dramatically during plastic deformation. Dislocations produce from existing dislocations, defects, grain boundaries and surface irregularities. Yield stress increases with increasing dislocation density and hence higher shear stress will be required for further motion of dislocations and consequentlely further plastic deformation. This process of strain hardening is easily observed during cold working of metals.

2.4.1 Dislocation density in cyclic loading

Considerable amount of work has been done in understanding the non-linear plastic relation between the stress and strain in a material loaded to an extent that dislocation movement is possible **[23]**. It can be understood that stress-strain relationship is closely related to the dislocation mean free path which can be defined as the average distance that the dislocations can move in the crystal before encountering an obstacle **[23].** In case of monotonic loading, dislocation density is known to increase with strain due to accumulation or piling-up of dislocations at the obstacles or the grain boundaries**[23**]. In case of cyclic loading, dislocation density changes due to the concept of dynamic recovery and its distribution changes from homogeneous to correlated structures like walls, channels, sub-cells and sub-grains etc. Hence the dislocation mean free path is also expected to change during cyclic loading. Thus the change

in dislocation density is required to be quantified for better understanding of mechanical behaviour of cyclically deformed steels.

Based on the mechanical behaviour during cyclic loading, materials are classified into two categories:

Cyclically softenable materials are the materials that soften upon cyclic loading. It implies that the stress required to produce same amount of strain in these materials decrease for every cycle. These materials are generally initially hard due to high forging stresses, prior cold work etc, and also the dislocation density is very high. During cyclic loading these materials show a decrease in overall dislocation density due to annihilation and redistribution of dislocations. This decrease in dislocation density causes cycle-dependent loss of strength which can be termed as cyclic softening.

Cyclically hardenable materials are generally initially soft and their dislocation density is low due to the annealing process that have undergone before cyclic loading [24]. During annealing treatment, annihilation of dislocations due to their increased mobility at high temperatures and long holding time periods [24]. During cyclic loading, accumulation of dislocations occurs due to incomplete reversal of the dislocations from the pile-ups [24]. This causes increase in dislocation density and it thereby causes a cycle-dependent strengthening of material known as cyclic hardening.

2.3.2 Calculation of dislocation density

Mechanical properties of metals are strongly dependent on dislocation density . The dislocation density in metals can be changed during cyclic loading. Techniques like XRD profile analysis

and hardness testing are used in calculating dislocation density. The method applied for estimating dislocation density through XRD profile analysis is by using Williamson- Hall plot.

Another method of estimating dislocation density is by using Vickers hardness data. In many experiments hardness of crystalline materials decreases with increasing load values which is known as Indentation size effect (ISE) [16]. In other materials reverse indentation size effect (RISE) was also observed where hardness increases with increasing load values.

CHAPTER 3

QUANTITATIVE ESTIMATION

3.1 Volume fraction Calculation using X-ray diffraction profile analysis

It is well known that upon plastic deformation austenitic phase transforms to martensite. So after deformation of austenitic stainless steel by cyclic loading, the specimens will have 2 phases in them- FCC austenite (γ) and BCT martensite(α'). For estimation of dislocation density of cyclically deformed austenitic stainless steel by X-Ray diffraction profile analysis, it is needed to consider dislocation densities associated with both γ and α' peaks.

For calculation of volume fraction of phases, X-Ray diffraction analysis is required. Volume fraction and intensity for different peaks can be given by: [18] –

$I_i^{hkl} = CR_i^{hkl} V_i / 2\mu$

where,

$$C = \left(\frac{I_0 A \lambda^3}{32\pi r}\right)\left[\left(\frac{\mu_0}{4\pi}\right)\frac{e^4}{m^2}\right] \quad \text{and,}$$

$$R_{hkl} = \left(\frac{1}{\upsilon^2}\right)\left[|F|^2 \; p\left(\frac{1+\cos^2 2\theta}{\sin^2\theta\cos\theta}\right)\right]\left(e^{-2M}\right)$$

For a steel containing austenite (γ) and bcc martensite (α'), above stated equation can be written as

$I = KR_\gamma V_\gamma / 2\mu$

$I = K R_{\alpha'} V_{\alpha'} / 2\mu$

Additionally

$V_\gamma + V_\alpha = 1$

Volume fraction is obtained by the formula

$$V_i = \frac{\frac{1}{n}\sum_{j=1}^{n}\frac{I_i^j}{R_i^j}}{\frac{1}{n}\sum_{j=1}^{n}\frac{I_\gamma^j}{R_\gamma^j}+\frac{1}{n}\sum_{j=1}^{n}\frac{I_{\alpha'}^j}{R_{\alpha'}^j}}$$

Where,

i = γ or α' in this instance and n is the number of peaks examined.

The above equation gives volume fraction of austenite and martensite in cyclically deformed austenitic stainless steel from a XRD profile analysis.

3.2 Estimation of dislocation density

For assessment of dislocation density in cyclically deformed non-conventional austenitic stainless steel i.e. X12CrMnNiN17-7-5 according to ISO/TR 15510:1997 [2], two methods were adopted-

1- X-Ray diffraction profile analysis
2- Hardness test (Indentation Size effect)

3.2.1 X-Ray diffraction profile analysis

Assuming that dislocation density causes strain broadening, the full width half maximum (FWHM) of diffraction profiles can be given by the modified Williamson–Hall plot [19]

$$\Delta K \cong 1/d + \left(\frac{\pi M^2 b^2}{2}\right)\rho^{1/2}\left(K^2\overline{C}\right) + O\left(K^4\overline{C}^2\right)$$

$\overline{C}$ represents the average value of contrast factor of dislocations for a particular reflection. It has been shown that in the cubic crystal system the average contrast factors are a linear function of the fourth-order invariant of the hkl indices of the different reflections.[15].

$\overline{C} = \overline{C}_{h00}(1 - qH^2)$,

Where $H^2 = (h^2k^2 + k^2l^2 + h^2l^2)/(h^2+k^2+l^2)^2$ and $\overline{C}_{h00}$ is the average contrast factor corresponding to h00 reflection.

3.2.2 Calculation of $\overline{C}_{h00}$ for FCC and BCC crystals

$\overline{C}_{h00} = a\,[1-\exp(-A_i/b)] + c\,A_i + d$

Where a, b, c and d are constants varies with type of dislocations and crystals.

The values of q in FCC and BCC crystals

$q = a\,[1-\exp(-A_i/b)] + c\,A_i + d$

Where a, b, c and d are constants varies with type of dislocations and crystals.

Total dislocation density of cyclically deformed austenitic stainless steel is given by

$= \rho_\gamma V_\gamma + \rho_{\alpha'} V_{\alpha'}$

Where ρ_γ and $\rho_{\alpha'}$ are dislocation densities associated with γ and α' peaks respectively.

3.2.3 Vickers hardness test (Indentation size effect)

For estimation of dislocation density of cyclically deformed non-conventional austenitic stainless steel, Vickers hardness test can also be used. Crystalline materials often show a discrete transition from elastic to plastic deformation upto critical indentation depth. The initially very high plastic hardness decreases until, at an indentation depth of larger than 10 μm. This is referred to as indentation size effect. [17]. The indentation size effect which is observed during

hardness testing of crystalline materials has been modeled in terms of GNDs (geometrically necessary dislocations) using a corrected Nix/Gao model by Durst et al.[17]. As the indenter is forced into the surface of a single crystal, geometrically necessary dislocations are required to account for the permanent shape change at the surface. There are other dislocations also known as statistically stored dislocations which are responsible for resistance to indentation. The indentation depth is denoted by h*, b is the magnitude of the Burgers vector, V the storage volume of the GNDs, and Θ is the angle between the surface and the indenter.

$$\rho_{GND} = \frac{3\tan^2\theta}{2f^3bh^*}$$

where f is correction factor. f= 1.9 for Vickers indenter.

The statistically stored dislocation density (ρ_s) is obtained from uniaxial stress–strain data applying the Tabor concept of the representative strain. [17]. Note that ρ_s is not expected to depend on the depth of indentation. Rather it depends on the average strain in the indentation, which is related to the shape of the indenter (tan θ)[16]

$$\frac{H}{H_0} = \sqrt{1+\frac{h^*}{h}}$$

where $$H_O = 3\sqrt{3}\alpha\mu b\sqrt{\rho_s}$$

here α = constant

μ= shear modulus

b= bergers vector

Total dislocation density would be given by

$$\rho_T = \rho_{GND} + \rho_s$$

Comparison between the dislocation density values obtained in XRD profile analysis and hardness test method is done and validation of both the methods can be verified.

CHAPTER 4

EXPERIMENTAL PROCEDURE

4. EXPERIMENTAL PROCEDURE

4.1 Introduction

The objective of this investigation is to study sub-structural changes in austenitic stainless steel due to strain controlled cyclic loading i.e. low cycle fatigue and dislocation density assessment after deformation. Experiments which were conducted for the study are described in this chapter. An overview of this chapter includes material selection, heat treatment, microstructural characterization, low cycle fatigue tests by varying strain amplitudes, determination of phase transformation by X-Ray diffraction profile analysis, estimation of dislocation density using X-Ray diffraction profile analysis and using Vickers hardness test.

4.2 Material Selection

Non-conventional austenitic stainless steel also called as X12CrMnNiN17-7-5 according to ISO/TR 15510:1997 [2] was selected for this experiment. It is commercially pure in nature. As-received material was in the rod-shape having diameter 16mm.

4.3 Heat Treatment

Procurement of selected material was done from market so previous deformation history of samples is unknown. Thus it is necessary to eliminate any residual stresses present in material. For this, solution annealing which assists in dissolution of any precipitated carbide phases at elevated temperature was done. These precipitated carbide phases may decrease corrosion

resistance. This heat treatment i.e. solution annealing includes heating the steel samples at 960^{o}C for 1 hour followed by water quenching.

4.4 Metallography

At first sample preparation is needed for microstructural studies. Cylindrical samples of height 12mm were cut using hack saw from heat treated rods. The samples were polished according to the standard metallographic route for polishing. For diamond polishing, diamond paste was applied on rotating wheel covered with special cloth to obtain 0.25μm surface finish. Etching of polished specimens was done using aqua regia solution [25% HNO_3 and 75% HCl).

4.4.1 Optical Microscopy

Microstructure of the polished specimens were obtained by optical microscope (Model: Zeiss LSM700, Germany) and images were captured at different magnifications.

4.4.2 Grain Size Measurement

The grain size of the solution annealed non-conventional austenitic stainless steel specimens was determined using linear intercept method according to ASTM E-112 [28].

d = length of the line / number of intercepts (4.1)

4.5 Hardness Determination

Hardness of the solution annealed and polished specimens of austenitic stainless steel was determined by using a Vickers Microhardness Indenter (Model: Leco LV 700, USA). An indentation load of 50gf was taken for hardness tests.

4.6 Low cycle fatigue tests

Strain controlled low cycle fatigue experiments of specimens of non-conventional austenitic stainless steel having diameter of 6 mm and gauge length of 12.5 mm were carried out at room temperature using universal servo-hydraulic BISS testing machine by Upadhyay et al. [26]. 3 samples of the low cycle fatigue experiment conducted by Upadhyay et al.[26] were taken for estimation of dislocation density.

Table 3.1 Test Matrix for Low cyclic fatigue tests Upadhyay et al. [supriya]

Material: **ISO/TR 15510 X12CrMnNiN17-7-5 SS**			
Sample No.	Strain Amplitude (%)	Strain rate (s^{-1})	Frequency (Hz)
1	±0.30	$5x10^{-3}$	0.417
2	±0.45	$5x10^{-3}$	0.278
3	±0.65	$5x10^{-3}$	0.192

4.7 X-ray Diffraction (XRD)

Quantitative and qualitative phase analysis of transformed phases, estimation of dislocation density and dislocation character can be performed by XRD profile analysis. Deformed specimens were cut from the gauge region using wire EDM cutter into cylindrical specimens of height 2mm. Samples were subjected to XRD in the scanning range of 40°- 110° and scanning rate of 5°/min.

4.8 Hardness test of deformed specimens

For estimating dislocation density, it is required to obtain hardness values at various loads. Cylindrical deformed specimens were polished using series of emery papers 3/0 and 4/0 for obtaining accurate results. Hardness tests were done by using Vickers Hardness tester at various loads i.e. 1kgf, 3kgf, 5kgf, 10kgf and 20kgf. Dwell time was 10seconds. 3 readings for each load were taken for each sample.

CHAPTER 5

RESULTS & DISCUSSION

Introduction

This chapter consists of the results obtained in the experiments mentioned in Chapter 4. The chapter is divided into various sub-sections: Section 5.1 includes the microstructural analysis of non-conventional austenitic stainless steel sample. Section 5.2 contains the hardness test results for the as-received sample. Section 5.3 includes typical results of low cycle fatigue tests done by Upadhyay et al.[ref]. Section 5.4 contains results of XRD test (XRD peaks) and also results of volume fraction calculations, dislocation density and character calculations. It also contains various plots related to dislocation density and volume fractions. Section 5.5 contains the result of hardness test of the cyclically loaded samples and also contains the calculation of dislocation density from hardness. It also contains various plots related to hardness test results. All these results are suitably discussed and a correlation of strain amplitude, dislocation density and character of dislocations are made. The chapter is ended with comparison between the dislocation densities obtained by XRD and hardness tests.

5.1. Microstructural analysis

Micrographs reveals that the steel contains equi-axed austenite grains. A typical micrograph of the sample is shown in the figure below. Grain size was calculated from the optical micrographs by linear intercept method: ASTM E112 [27]. Average grain size of the sample was found to be 43.69± 2.3 μm.

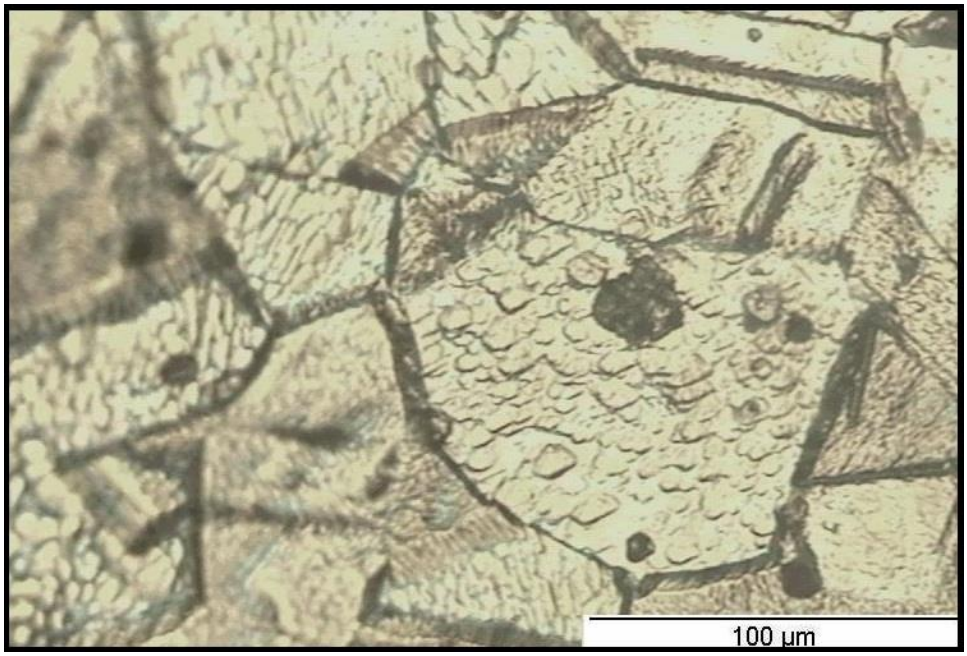

Fig.5.1. Optical Micrograph of non-conventional austenitic stainless steel

5.2. Hardness Measurement

Micro-Hardness test of the as-received non-conventional stainless steel was conducted at a load of 50gf and dwell time of 15 seconds in a Micro-hardness tester. Five readings were taken for each sample at different positions. Average hardness of these are calculated and the obtained value was 231±3.6 HV.

5.3. Low cycle Fatigue analysis

Typical results are shown as plots between max/min stresses versus number of cycles in Fig. 5.2. The strain rate is taken to be 5×10^{-3} and the strain amplitude was varied as ±0.3%, ±0.45%, ±0.65%. It can be observed that with increasing number of cycles, the maximum stress is increasing and minimum stress is decreasing. This phenomenon shows that non-conventional austenitic stainless steel is cyclically hardenable material.

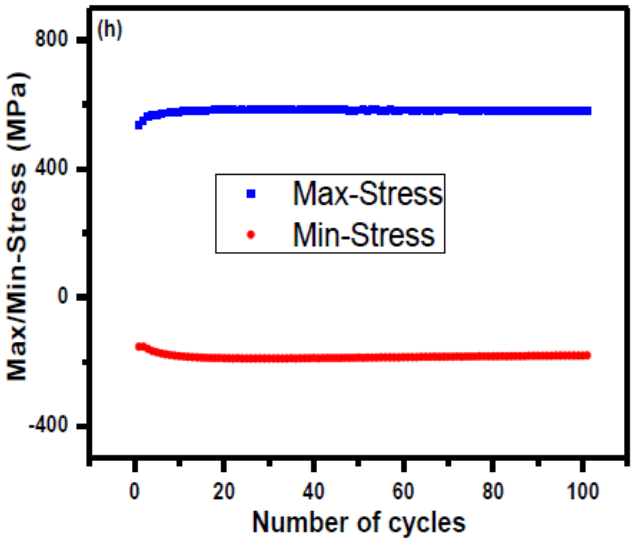

Fig 5.2. A typical plot showing response of maximum/minimum stress with number of cycles at a strain amplitude of ±0.65, up to 100 cycles at ambient temperature. (Supriya et al.[26])

5.4. X-Ray Diffraction profile analysis

X-ray diffraction experiments were conducted at a step size of 5^{o}/min with angle ranging from 40^{0} to 110^{0}. Fig.5.3 shows the XRD profile for the as-received non-conventional austenitic stainless steel sample. Since the as-received is undeformed, it contains only γ austenite phase and hence its XRD profile contains only γ peaks but no α' peaks.

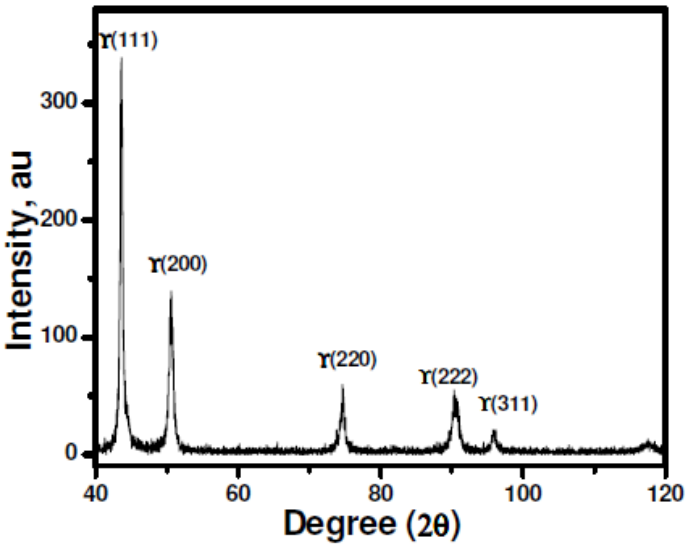

Fig.5.3. XRD profile for undeformed specimen showing indexed γ peaks [28]

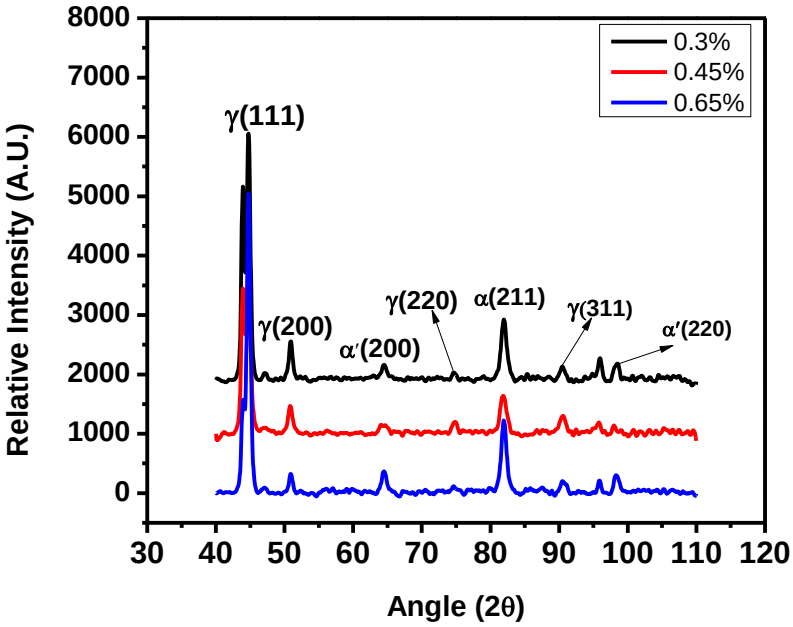

Fig.5.4. XRD profiles of cyclically loaded samples at various strain amplitudes ±0.3%, 0.45%, 0.65%.

In Fig.5.4, X-ray peaks obtained were indexed which revealed the presence of α' martensite and γ austenite phases. α'martensite was formed as a result of strain induced transformation in which the energy required for the transformation of austenite to martensite is provided by the plastic deformation. The relative intensity and angle values are used for calculation of volume fractions and dislocation densities of various phases.

5.4.1 Estimation of volume fraction of α' martensite

Both monotonic and cyclic deformation induces phase transformation in austenitic stainless steel [2]. Thus X12CrMnNiN17-7-5 steel is metastable on deformation. After performing X-Ray diffraction experiment on specimens which were cyclically deformed under ±0.3%, ±0.45% and ±0.65% strain amplitudes, peaks of α' martensite (BCC) and γ austenite (FCC) were obtained (Fig5.4). There are very few literature works which discussed about phase transformation of cyclically deformed austenitic stainless steel under various constant strain amplitudes and volume fraction of the transformed phases associated with it. C.Müller et al. studied about fatigue behavior of austenitic stainless steel and concluded that endurance limit is greatly affected by martensite formation under dynamic loading and sensitivity of endurance limit towards test conditions also get incremented.

Table5.1 Calculated volume fraction of α' martensite and γ austenite from XRD profile analysis

S. No	Strain amplitude	Volume fraction of γ	Volume fraction of α'
1	± 0.3%	0.688	0.312
2	± 0.45%	0.678	0.322
3	± 0.65%	0.671	0.329

From Table 5.1 and Fig. 5.5, it was observed that with increase in strain amplitude, volume fraction of α' martensite increases. As received sample was completely austenitic and there was no martensitic phase but on application of cyclic loading under constant strain amplitudes, strain induced transformation takes place and α' martensite formed and increased with strain. Here, the driving force for the strain induced transformation is the strain energy absorbed during deformation of material. As the strain amplitude increases the absorbed strain energy increases and hence the amount of martensite formed also increases.

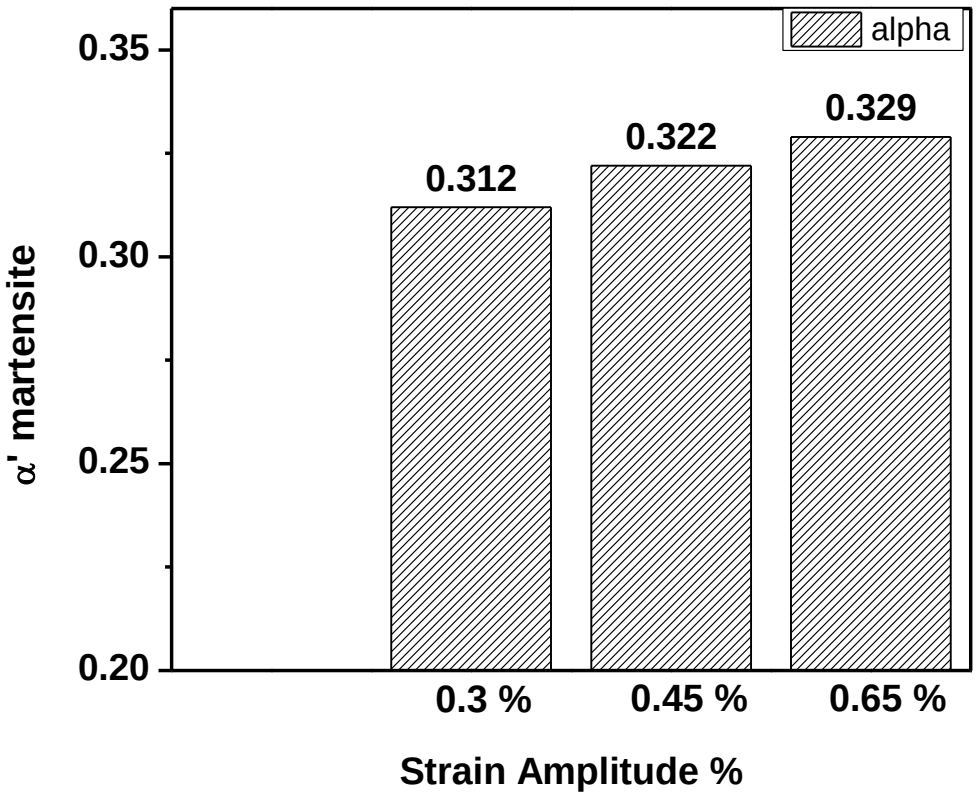

Fig 5.5. Plot showing volume fraction of α' martensite phase against different strain amplitudes.

Calculation of volume fraction of α' martensite and γ austenite also assists in calculation of dislocation density using X-Ray diffraction profile analysis. For calculating total dislocation

density of material, we can calculate weighted sum of dislocation densities associated with α' and γ peaks multiplied with their volume fraction respectively.

5.4.2. Estimation of dislocation density through X-Ray profile analysis:

Dislocation density from X-Ray profile can be obtained by using the modified Williamson-Hall equation [25]. Broadening of the peaks in X-Ray profile occurs due to the dislocations generated during cyclic loading. Dislocation density of various planes in both α' and γ phases can be related to the full width at half maximum of the respective α' and γ peaks. The Williamson-Hall equation can be given as

$$\Delta K \cong 1/d + \left(\frac{\pi M^2 b^2}{2}\right)\rho^{1/2}\left(K^2\overline{C}\right) + O\left(K^4\overline{C}^2\right)$$

As mentioned in chapter 3, For C_{h00} calculation, elastic anisotropy A_i is obtained from the formula:

$$A_i = 2C_{44} / (C_{11} - C_{12})$$

For Iron, the values the three elastic constants, C_{11}, C_{12}, C_{44}, are given as C_{11} = 237GPa, C_{12} = 141GPa, C_{44} = 116GPa **[3]**. The values of a, b, c, d required for the calculation of C_{h00} is obtained by considering the value of C_{12} / C_{44} which is approximately equal to one for Iron. Accordingly the values of a, b, c, d in C_{h00} calculation for screw and edge dislocations for both bcc and fcc crystals are tabulated in Table 5.1:

Table.5.2: The values of a, b, c, d in C_{h00} calculation for screw and edge dislocations for both bcc and fcc crystals.

	FCC crystal		BCC crystal	
	Screw dislocation	Edge dislocation	Screw dislocation	Edge dislocation
a	0.1740	0.1687	0.1740	1.6690
b	1.9522	2.04	1.9522	21.124
c	0.0293	0.0194	0.0293	0
d	0.0662	0.0926	0.0662	0.0757

Similarly the values of a, b, c, d required for calculation of q obtained by considering C_{12} / C_{44} which is approximately equal to one for Iron are tabulated in Table 5.2.

Table.5.3. The values of a, b, c, d in q calculation for screw and edge dislocations for both bcc and fcc crystals.

	FCC crystal		BCC crystal	
	Screw dislocation	Edge dislocation	Screw dislocation	Edge dislocation
a	5.4252	4.8608	8.6590	7.2361
b	0.7196	0.8687	0.3730	0.9285
c	0.0690	0.0896	0.0424	0.1359
d	-3.1970	-3.4280	-6.074	-5.7484

The value of average contrast factor C is calculated from the values of C_{h00} and q for various peaks. Screw and Edge dislocation densities were calculated for different peaks using

Williamson-Hall equation [25]. Total dislocation densities for each peak were calculated by summing up the obtained screw and edge dislocation densities. The results are shown in Table 5.3.

Table.5.4. The values of screw, edge and total dislocation densities associated with various peaks for specimens cyclically loaded at different strain amplitudes.

Strain amplitude	**Peaks indexed**	**Average ρ_{screw} (m^{-2})**	**Average ρ_{edge} (m^{-2})**	**Average ρ_{total} (m^{-2})**
±0.3%	**α'** (110), (200), (211), (220)	1.64×10^{14}	0.69×10^{14}	2.085×10^{14}
	γ (111), (200), (311).	3.05×10^{14}	1.07×10^{14}	4.10×10^{14}
±0.45%	**α'** (110), (200), (211), (220)	4.21×10^{14}	1.08×10^{14}	5.29×10^{14}
	γ (111), (200), (220), (311).	11.5×10^{14}	3.06×10^{14}	14.57×10^{14}
±0.65%	**α'** (110), (200), (211), (220)	5.56×10^{14}	1.41×10^{14}	6.97×10^{14}
	γ (111), (200), (220), (311).	14.48×10^{14}	3.70×10^{14}	18.18×10^{14}

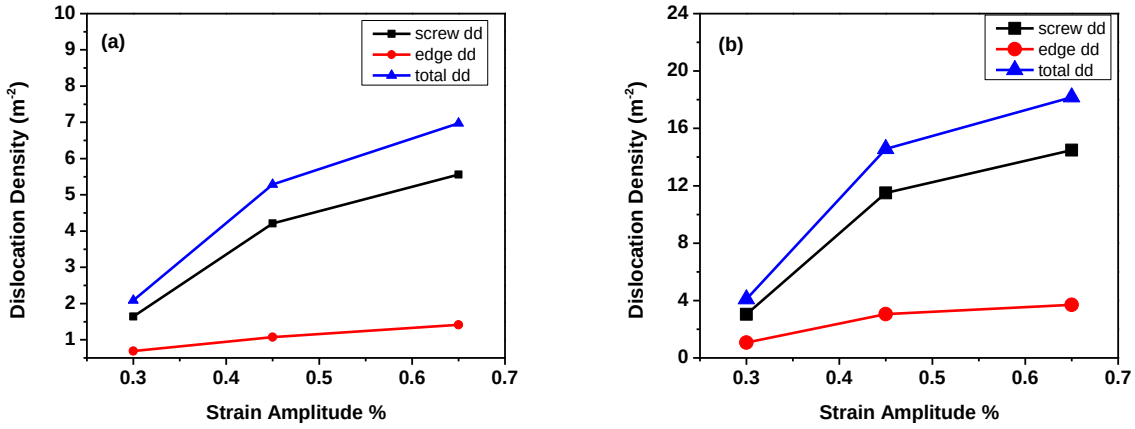

Fig 5.6. Plots showing edge, screw and total dislocation densities for different strain amplitudes for a) α' peaks b) γ peaks.

Fig 5.6 shows that with increasing strain amplitudes edge, screw and total dislocation densities increase in both α' and γ peaks. The reason for this can be given from the fact that non-conventional austenitic stainless steel is cyclically hardening material. It can also be noted that the screw dislocation density is greater than edge dislocation density in both the plots. Stainless steel is a material with moderate stacking fault energy value. Therefore during deformation, a part of the generated screw dislocations can cross slip which produces regions of high screw dislocation density by multiplication.

The screw, edge and total dislocation densities for the samples including the values for both α' and γ peaks are obtained by doing a weighted sum of dislocation densities multiplied with the volume fractions of the respective phases. The results are shown in Table 5.5.

Table 5.5: The values of screw, edge and total dislocation densities considering both α' and γ phases for specimens cyclically loaded at different strain amplitudes.

Strain amplitude	ρ_{screw} (m^{-2})	ρ_{edge} (m^{-2})	ρ_{total} (m^{-2})
±0.30%	2.61×10^{14}	0.95×10^{14}	3.56×10^{14}
±0.45%	9.15×10^{14}	2.42×10^{14}	11.57×10^{14}
±0.65%	11.54×10^{14}	2.95×10^{14}	14.49×10^{14}

5.4.2. Evaluation of dislocation character:

Percentage of edge and screw dislocations in the total dislocations can be obtained by dividing them and the results are tabulated in Table 5.6.

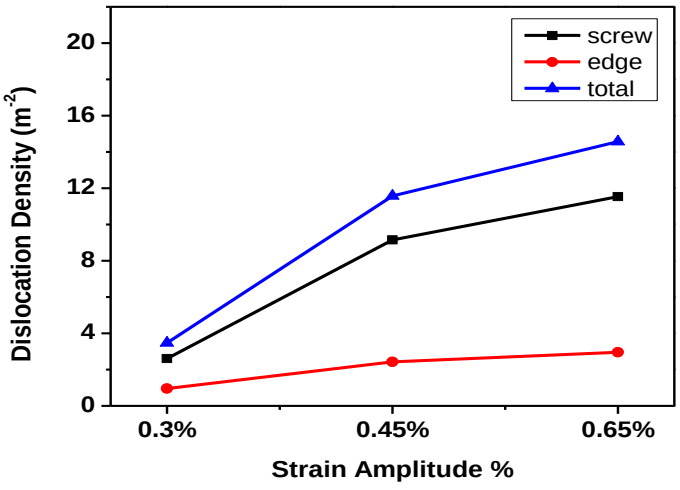

Fig 5.7. Plot showing edge, screw and total dislocation density for the three samples by combining α' and γ peaks using volume fractions of α' martensite and γ austenite phases.

Table 5.6. Percentage Screw and Edge dislocations for different strain amplitudes

Strain Amplitude	% Screw dislocations	% Edge dislocations
±0.3%	73.3%	26.7%
±0.45%	79.1%	20.9%
±0.65%	79.6%	20.35%

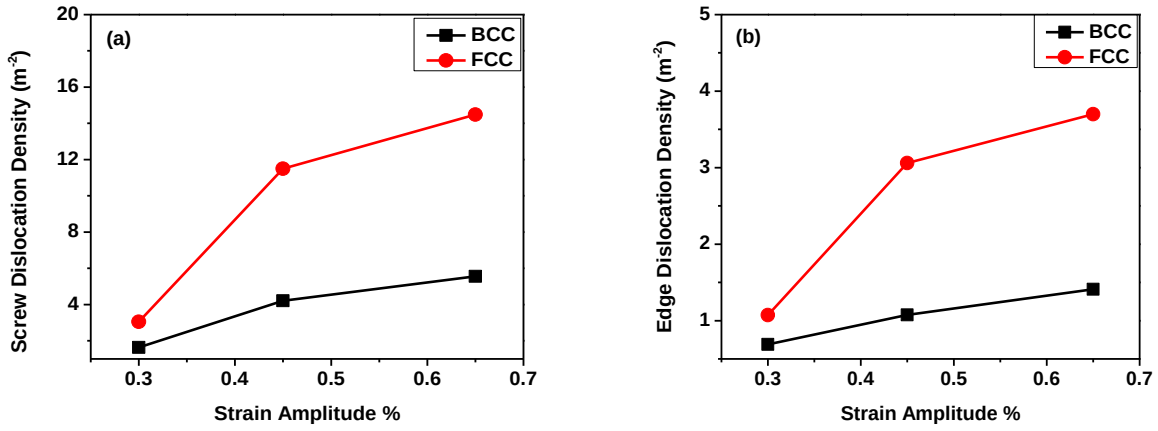

Fig 5.8. Plots showing a) screw dislocation density b) edge dislocation density, of different samples in α' martensitic (BCC) and γ austenitic phases (FCC).

In Fig 5.8 it can be seen that both screw and edge dislocations are more in FCC (γ austenite) than in BCC (α' martensite).

5.5. Hardness determination of deformed specimens:

Hardness values of the specimens, cyclically deformed in low cycle fatigue experiment at constant strain amplitudes of ±0.3%, ±0.45% and ±0.65%, were determined at various loads.

Table 5.7 Mean hardness values at different loads

S.NO	Load(kgf)	Mean Hardness (HV)		
		±0.3% strain amplitude	±0.45% strain amplitude	±0.65% strain amplitude
1	1	437.067	465.133	513.533
2	3	427.967	456.8	507.267
3	5	384.3	450.4	485.43
4	10	410.67	446.167	516.5
5	20	388.767	440.7	484.367

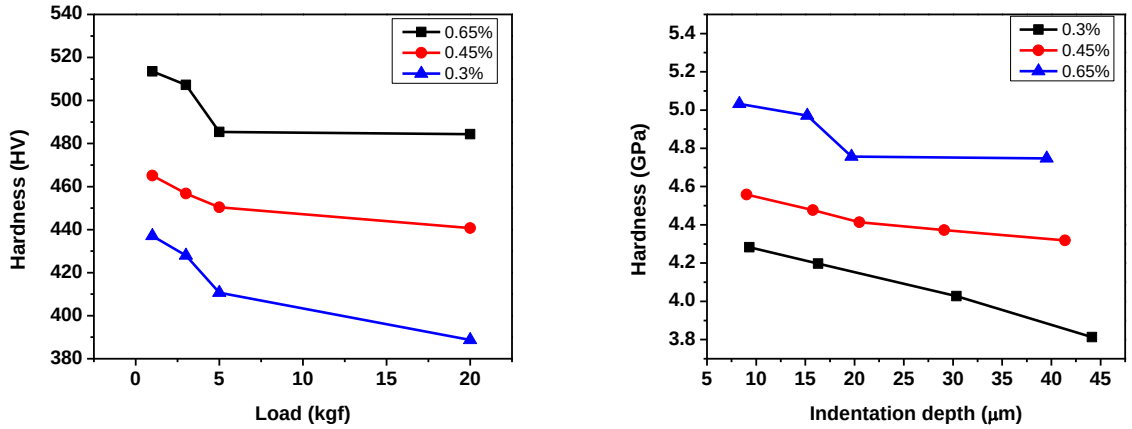

Fig 5.9. Plots illustrating Indentation size effect a) Hardness number (HV) vs Load (kgf) and b) Hardness (GPa) vs Indentation depth (μm).

In the Fig5.9. it is observed that with increasing indentation load, mean hardness value of specimen, deformed under particular strain amplitude, decreases. This phenomenon is known as indentation size effect. Crystalline materials often show an intrinsic transition (pop-in) from elastic to plastic deformation up to certain indentation depth in micrometers. This pop-in behavior occurs because once the shear stress underneath the indenter has reached the theoretical strength of the material, dislocation nucleation and spreading must occur. Thus plastic zone is formed due to nucleation of large amount of geometrically necessary dislocations (GNDs). Before this pop-in statistically stored dislocations are responsible for hardness which is depth independent, after pop-in GNDs are responsible for hardness which is depth dependent. Plastic zone formation lowers the hardness value.

5.5.1 Evaluation of dislocation density by the model of indentation size effect

If we draw the plot of log(P) Vs log(d), its slope value will help in distinguishing between indentation size effect and reverse indentation size effect, where P is indentation load and d is average diagonal length of indentation. According to Meyer law;

$$P = kd^{n'}$$

Where P= applied load, kgf

d = diameter of the indentation, mm

n’ = a material constant related to strain hardening of metal

k = material constant showing resistance to penetration.

Slope of log(P) vs log(d) gives value of n’. slope can be determined by doing linear fit of the plot.

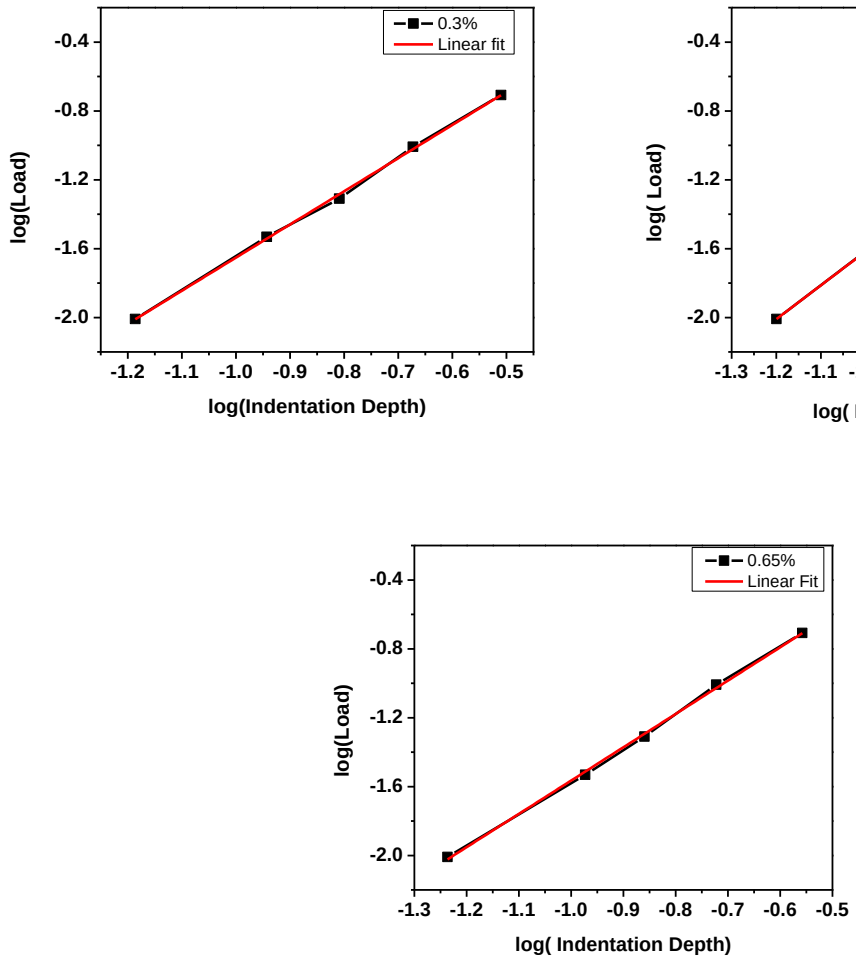

Fig 5.10 . Plots showing the log (P) vs log (d) and their linear fits for a) ±0.3% strain amplitude b) ±0.45% strain amplitude c) ±0.65% strain amplitude.

Table 5.8 n' values for different specimens cyclically deformed under various strain amplitudes

S NO.	Strain amplitude (%)	Slope value or n
1	±0.3	1.9256
2	±0.45	1.9653
3	±0.65	1.9345

Since n'<2 for all strain amplitudes, it can be concluded that deformed specimens are showing indentation size effect [16].

5.5.2. Model of indentation size effect

For crystalline materials, indentation size effect can be modelled accurately using concept of geometrically necessary dislocations. The model leads to following equation for depth dependent hardness

$$\frac{H}{H_0} = \sqrt{1 + \frac{h^*}{h}}$$

Value of H_o can be obtained from the intercept value of H_v (GPa) Vs 1/h (mm^{-1}) plot using linear fit.

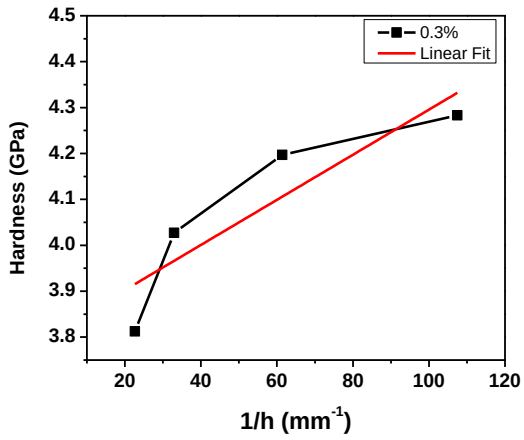

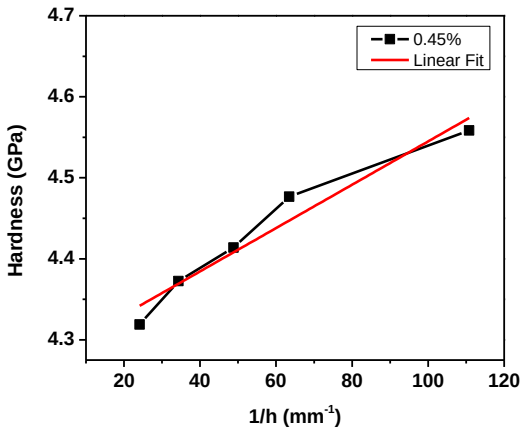

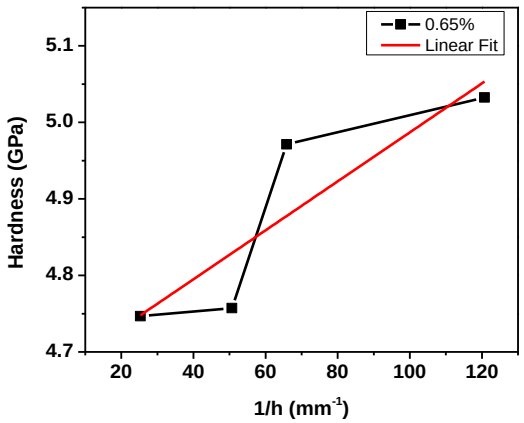

Fig 5.11 Plots showing Hardness (GPa) vs 1/h (mm^{-1}) and their linear fits for a) ±0.3% strain amplitude b) ±0.45% strain amplitude c) ±0.65% strain amplitude.

Table 5.9 H_o values obtained from H_v (GPa) Vs 1/h (mm^{-1}) plot

S NO.	Strain amplitude (%)	H_o (Gpa)
1	± 0.3	3.8043
2	± 0.45	4.2775
3	± 0.65	4.7908

For calculation of h*(mm), which is required to calculate density of geometrically necessary dislocations, slope of $(H/H_o)^2$ Vs 1/h plot was calculated using linear fit of plot.

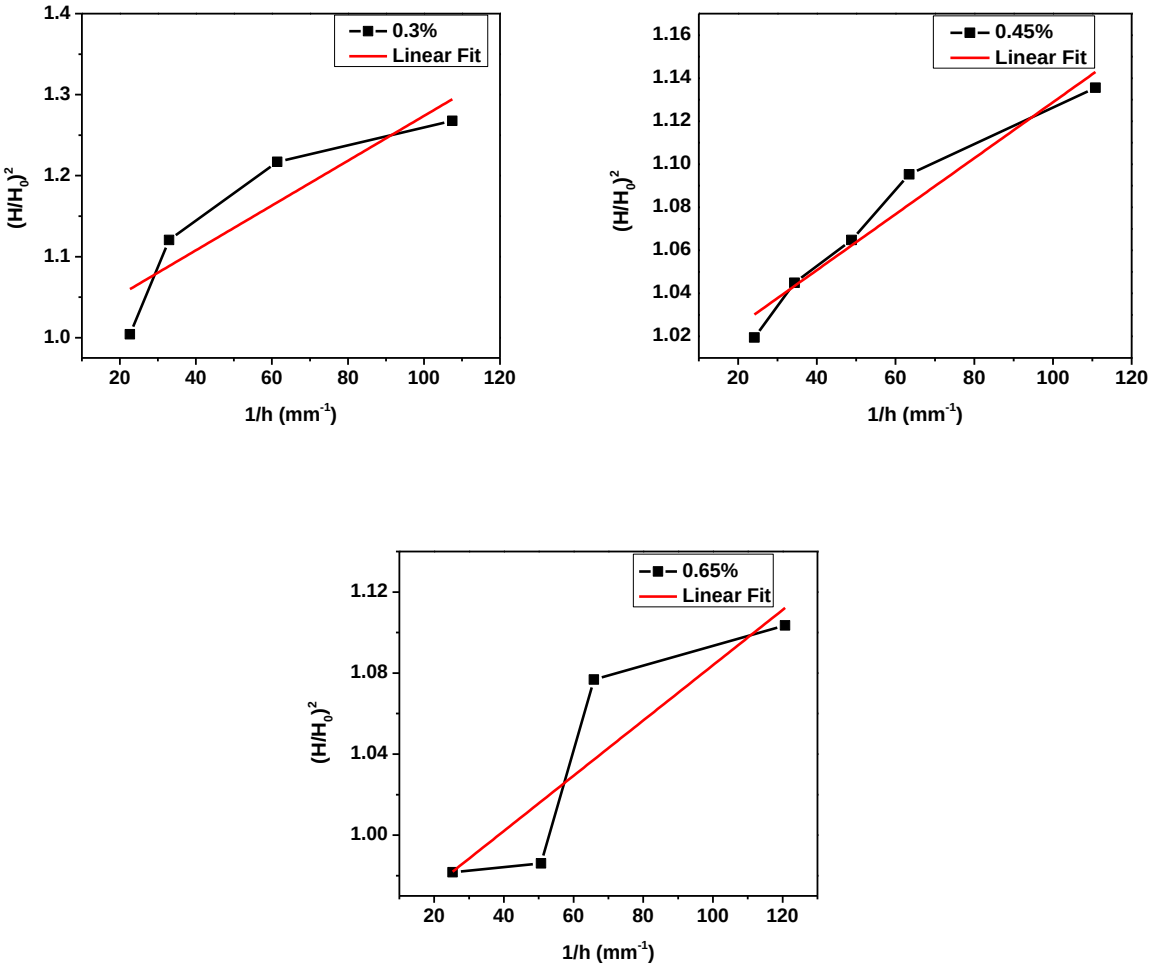

Fig 5.12 Plots showing $(H/H_o)^2$ vs 1/h and their linear fits for a) ±0.3 % strain amplitude b) ±0.45% strain amplitude c) ±0.65% strain amplitude.

Table 5.9 h* values obtained from $(H/H_o)^2$ Vs 1/h plot

S NO.	Strain amplitude (%)	h* (mm)
1	±0.3	0.0028
2	±0.45	0.0013
3	±0.65	0.0009

5.5.3 Calculation of dislocation density

The density of geometrically necessary dislocations (ρ_{GND}) was calculated using corrected Nix/Gao model.

$$\rho_{GND} = \frac{3\tan^2\theta}{2f^3bh^*}$$

The statically stored dislocation densities of all specimens deformed under various constant strain amplitude were also calculated.

Total dislocation density (ρ_{total}) of deformed specimen is algebraic sum of ground necessary dislocation density and statically stored dislocation density.

Table 5.10 Calculated ρ_{GND} , ρ_{SSD} and ρ_{Total} of specimens cyclically deformed at various strain amplitudes

S.No	Strain amplitude	ρ_{GND} (m^{-2})	ρ_{SSD} (m^{-2})	ρ_{Total} (m^{-2})
1	±0.3	0.506×10^{14}	5.786×10^{15}	5.8366×10^{15}
2	±0.45	1.09×10^{14}	7.315×10^{15}	7.424×10^{15}
3	±0.65	1.57×10^{14}	9.1759×10^{15}	9.3329×10^{15}

5.5.4 Effect of strain amplitude on dislocation density:

From Fig 5.13 It is quite clear that with increase in strain amplitude, dislocation density of deformed specimens increases. This establishes that the material taken is cyclically hardening.

Increase in dislocation density implies that the stress required for deformation increases and hence cyclically hardens.

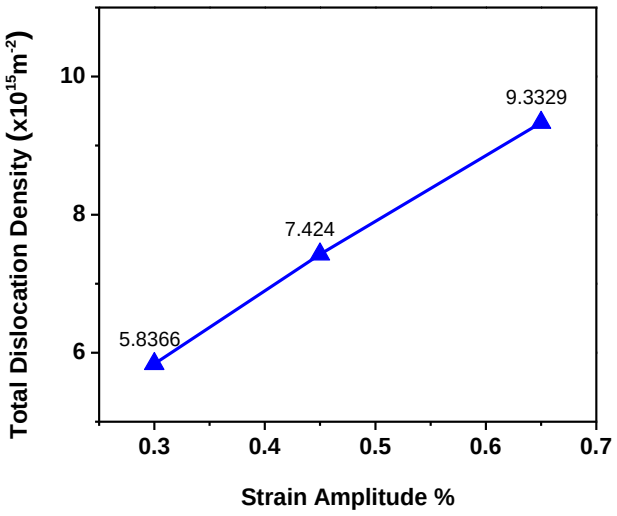

Fig 5.13 Plot showing total dislocation density obtained by summing GNDs and SSDs against different strain amplitudes.

5.5.5 Comparison between dislocation densities obtained by XRD profile analysis and hardness test:

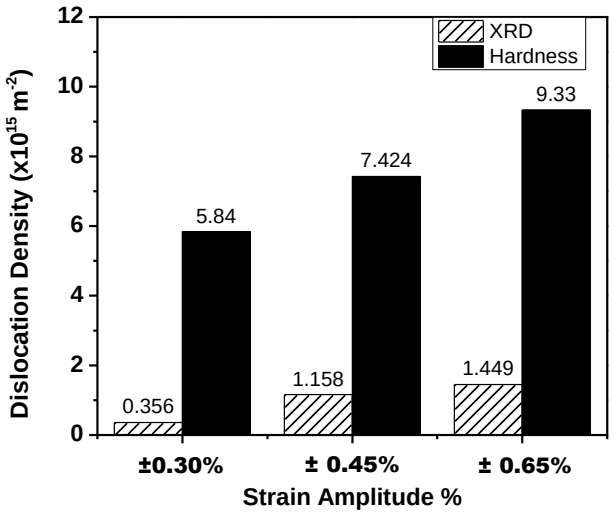

Fig 5.14 Plot showing a comparison of dislocation densities obtained for different strain amplitudes using X-ray profile analysis and hardness test values.

Fig 5.14 shows that the dislocation densities obtained by both XRD profile analysis and hardness test values increase with an increase in strain amplitude. It can be observed that the dislocation densities obtained by XRD profile analysis are lesser than the values obtained from hardness tests. This may be due to elimination of few peaks in XRD profile which have very small intensities during softening of the XRD profile. Also some more peaks of smaller intensities may have been revealed if the step size was lesser.

CHAPTER 6

CONCLUSIONS

CONCLUSIONS:

XRD profile analysis using modified Williamson-Hall plot has been carried out to estimate dislocation densities and character in the specimens subjected to cyclic loading at different strain amplitudes. A correlation between the dislocation densities and strain amplitudes has been established. The same investigations were carried out using hardness test approach and the results obtained from both the approaches were compared for consistency. Conclusions made from the results of the present investigation:

1) X-ray diffraction profile analysis can be used in estimating dislocation densities and character of deformed specimen. The results were consistent and as expected, the dislocation density increased from 3.56 $x10^{14}$ to 14.49 $x10^{14}$ with increase in strain amplitude from ±0.30% to ±0.65%.
2) It can be concluded that the percentage of screw dislocations is greater than percentage of edge dislocations in both α' (martensite) and γ (austenite) phases.
3) XRD profile analysis showed that the material has undergone strain induced martensitic transformation during cyclic loading and the amount of martensite formed has increased with increase in strain amplitude.
4) It can also be concluded that the non-conventional stainless steel shows indentation size effect as the hardness values showed a decrease with increase in load.
5) Dislocation density calculated from hardness values also showed an increase with increase in strain amplitude and it was in the same order as that of the dislocation density obtained from X-ray diffraction profile analysis.

6) It can be concluded that hardness test can be used as an efficient tool in calculating the dislocation density in deformed specimen as it showed consistent and expected trend in results.
7) From indentation size effect model calculations it can be concluded that the amount of statistically stored dislocations is greater than the amount of geometrically necessary dislocations.

FUTURE PROSPECTIVES OF THE WORK:

1) The estimation of dislocation density of cyclically deformed material can be performed using other techniques like transmission electron microscopy and the results can be compared.
2) Cyclic loading can be done by changing the test parameters like strain amplitude, strain rate, temperature etc and the results can be verified for consistency.
3) Comparative study of dislocation density estimated by different methods in cyclically loaded specimen can be done for different materials and the results can be verified if they are as per expectation.

REFERENCES:

[1] Bhadesia & Honeycombe, Steels: Microstructure & Properties, 3rd Edition, 2006

[2] A. Nayar , The Steel Handbook, Mc Graw Hill Publications, UK, 2001, 829–832

[3] Dieter, G. E.,, Mechanical Metallurgy, Singapore, McGraw-Hill Book Company, (1987).

[4] S. Suresh, Fatigue of materials, Cambridge University, 1998

[5] R.A. Renzetti, H. Sandim, R. Bolmaro, P. Suzuki, A. Moslang, Mater. Sci. Eng. A 534 (2012) 142–1462.

[6] S. Kalpakjian, Manufacturing Engineering and Technology, Wesley Publishing., 1995

[7] Properties and Selection of Metals,, Metals Handbook, 8th ed., ASM, 1961

[8] R. Higgins, Engineering Metallurgy— Physical Metallurgy, Arnold, 1993

[9] M.Meyers and K. Chawla, Mechanical Metallurgy—Principles and Applications, 1984

[10] C.M. Laird, ASTM, 1966, p 130

[11] R.W. Cahn, P. Haasen, Physical Metallurgy, Elsevier, North-Holland, 1996.

[14] T. Shintani, Y. Murata, Acta Materialia. 59 (2011) 4314–4322.

[15] T. Ungár, A. Borbély, Appl. Phys. Let. 69 (1996) 3173–3175.

[16] Nix; Gao, J. Mech. Phys. Solids, Vol. 46, No. 3, pp. 41 I-425. 1998

[17] Karsten Durst *, Bjorn Backes, Oliver Franke, Mathias Goken, Acta Materialia 54 (2006) 2547–2555

[18] De, A. K., Murdock, M Speer, J. G. and Matlock, Quantitative estimation of strain-induced martensite in 304 stainless steel by X-ray diffraction, Acta Materialia, Vol. 50, pp. 1445–1449.

[19] T. Ungár, Mater. Sci. Eng. A 309–310 (2001) 14–22.

[20] R. E. Smallman, R. J. Bishop, Physical Metallurgy Materials Engineering, Butterworth-Heinemann,

[21] Robert E.Reed-Hill, Physical Metallurgical Principles, second edition, D.Van Nostrand company

[22] Jeom-Yong Choi and Won Jin, Scripta Materialia, Vol. 36, No. 1, pp. 99-104, 1997

[23] T. Mayer , L. Balogh, Acta Materialia 60 (2012) 2485–2496,

[24] A. Das1, P. C. Chakraborti, Materials Science and Technology 2011 VOL 27 NO 1

[25] T. UngaÂ r,* I. Dragomir, J. Appl. Cryst. (1999). 32, 992±1002

[26] Supriya Upadhyay, K. Dutta, low cycle fatigue and post fatigue tensile behavior of a non-conventional stainless steel

[27] Standard Methods for Determining Grain Size,

Book of ASTM Standards, PA., ASTM, 03.01(2004): pp.E 112-0.

[28] Lopamudra Sahu, K. Dutta, Ratcheting of a Non-conventional austenitic stainless steel and it's Associated Microstructural Variations